Network performance analysis of a {PIC}-based reconfigurable add-drop multiplexer for multiband applications

Network Performance Analysis of a PIC-Based Reconfigurable Add-Drop Multiplexer for Multiband Applications

Muhammad Umar Masood[a], Lorenzo Tunesi[a], Ihtesham Khan[a], Bruno Correia[a], Enrico Ghillino[b], Paolo Bardella[a], Andrea Carena[a], and Vittorio Curri[a]

[a]Dipartimento di Elettronica e Telecomunicazioni, Politecnico di Torino, Corso Duca degli Abruzzi 24, Torino, Italy
[b]Synopsys, Inc., 400 Executive Blvd Ste 101, Ossining, NY 10562, United States

ABSTRACT

To reduce costs and simplify operations, network operators are deploying the latest network devices that are power efficient and compact. In this paper, a detailed comparison is made between the design of a reconfigurable add-drop multiplexer (ROADM) based on an integrated circuit (PIC) and the state-of-the-art ROADM devices. In particular, the performance of the device in terms of frequency response parameters is presented in the paper in comparison with the state-of-the-art ROADMs. The proposed PIC based ROADM can operate in a multi-band scenario, including C+L+S bands, and is potentially scalable to many output fibers and routed channels while maintaining a small footprint. A detailed network performance analysis is performed with the proposed PIC-based ROADM device and its impact on the network. Due to increasing traffic demand, the current optical transport infrastructure is experiencing capacity problems: two possible solutions are Spatial Division Multiplexing (SDM) and Bandwidth Division Multiplexing (BDM), which both allow capacity expansion of the existing infrastructure. We have studied the network performance of the proposed ROADM device on the Spain-E network and performed a detailed comparison for the SDM and BDM scenarios. Compared to the SDM approach, which requires the deployment of additional fiber, the cost-effective BDM scenario can better utilize capacity without installing new fiber infrastructure or using dark fibers.

Keywords: High capacity optical networks, Multi-band, Wavelength selective switch, Photonic integrated circuit, Network performance

1. INTRODUCTION

A larger optical network capacity is required due to the latest technologies, such as 5G and the Internet of Things (IoT), as well as the continued increase in global Internet traffic. Service providers want to expand their capacity, so they implement solutions that are inexpensive, scalable, and flexible. Modern optical transport achieves a maximum transmission rate of 38.4 Tbps per fiber using PM-16QAM by combining transparent wavelength division multiplexing (WDM) channel propagation and coherent dual polarization optical technology throughout the complete C-band in a spectral window of 4.8 THz.[1] It is necessary to implement solutions that either scale the technology that is currently in use or introduce new technologies in order to further enhance the capacity of the network. The most practical choices for increasing the capacity of optical networks are (a) spatial division multiplexing (SDM), which can be achieved using multicore (MCF), multimode (MMF), or multiparallel (MPF) fibers, and (b) band division multiplexing (BDM), which makes use of a wider spectral range of the fiber to permit transmission over the whole low-loss spectrum of optical fibers (e.g., 54 THz in ITU G.652).

The current SDM solutions rely on the introduction of additional fiber or the presence of dark fiber. However, replacement of the optical transport infrastructure requires a large CAPEX expenditure. BDM, on the other hand, leverages the fiber's unused spectral components to broadcast WDM channels spanning the whole low-loss spectrum, from the O to the L band (1260-1625 nm), with a possible total frequency bandwidth of over 50 THz.[2]

Further author information: muhammad.masood@polito.it

Transparent wavelength routing must also be enabled by the filtering and switching modules in order to use the BDM approach. The WSS, which independently controls and routes each input channel to a fiber output, is the key element of the WDM switching architecture. Microelectromechanical mirrors (MEMS) and liquid crystal on silicon (LCoS) technology are commonly used to construct WSS, producing in systems that are typically bulky and difficult to produce and maintain.[3] In contrast, the multi-band WSS implementation in this work makes use of the quickly evolving photonic integrated circuits (PICs) technology, which offers a low-cost, small-footprint, high-performance solution. The suggested WSS has a modular structure that enables it to function in a variety of optical spectrum bands, including the S+C+L bands. The proposed WSS has a lower footprint than existing MEMS-based systems and is scalable to take more output fibers and channels.

2. WSS ARCHITECTURE

The device under investigation consists of a WSS implemented through PICs designed for a DWDM multi-band implementation scenario. The proposed structure is capable of routing the given WDM channels independently in the S+C+L optical telecommunication windows, allowing non-blocking transparent wavelength-selective switching. The structure can be tailored to the desired number of channels, allowing custom design based on the envisioned transmission scenario, thanks to the modularity and scalability of the underlying architecture. These properties are enabled by the divide-and-conquer paradigm on which the structure is based, as depicted in Fig. 1: by separating the filtering operation from the switching operation, while the number of elements increases, flexibility and tunability can be improved.

Architecture and design principles are based on a previous architecture,[4,5] although the main channel filtering structure, implemented through Microring Resonators (MRRs), has been redesigned to improve the performance and accuracy of the model.

The first section aims to divide the WDM comb into its individual channels, simplifying the following switching operation; this is achieved through a cascade of different filtering elements, which first separates the three operational bands, allowing a finer division into the individual channels. Separation of the filtering process into multiple sub-stages is also necessary due to the envisioned application, targeting multi-band DWDM, which requires both extremely frequency selective components to reduce crosstalk and side-channel interference, while design flexibility over an ultra wide-band scenario (S+C+L). This is achieved through two main components, Contra-Directional Couplers (CDC)[6] and MRR-based two-stage ladder filters[7]. Regarding the default implementation of the two-stage ladder MRR elements used in the previous architecture, which uses standard directional couplers, the deployed model considers grating-assisted coupling regions[8], which are more suited for a dense

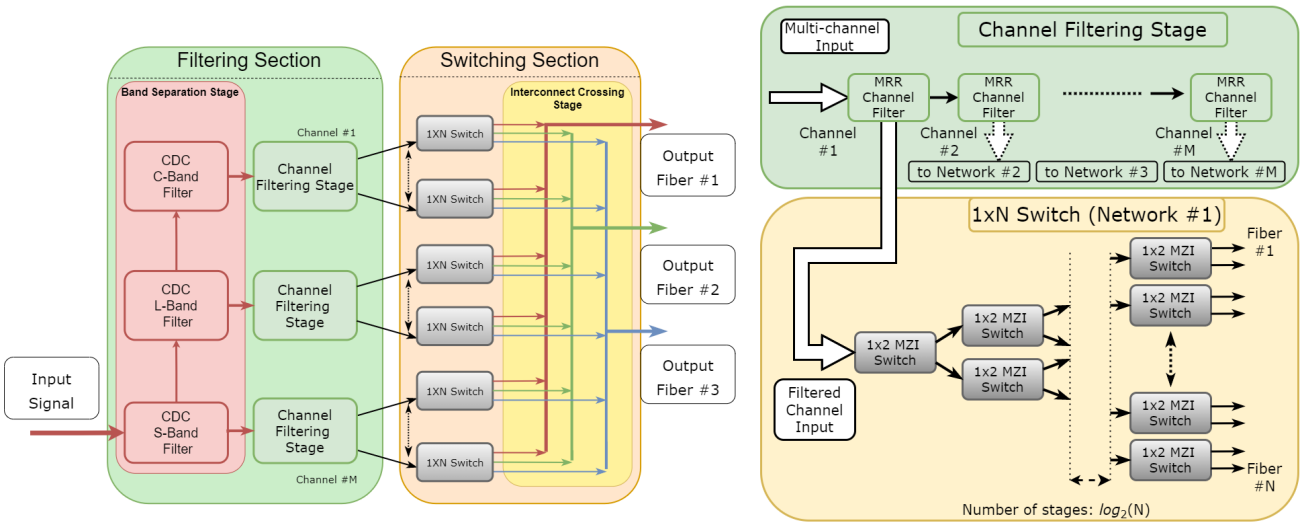

Figure 1: Proposed architecture for the WSS, highlighting the main functional blocks and their circuit representation.

WDM scenario and can better handle the aliasing normally introduced by MRR elements. This choice improves the scalability of the model and better accounts for the aliasing effect in the DWDM scenario.
Having separated each channel in an individual waveguide, the next section is tasked with switching and routing the signals to the target output ports. This operation is achieved by two stages: the routing is performed by a set of parallel binary tree switching networks, while the subsequent interconnect stage is tasked with combining and connecting the routed signals to the target output ports. The fundamental element used for the switching operation is the 1x2 Mach-Zehnder Interferometer (MZI), which can be controlled by applying an appropriate thermal shift between the arms. As in the previously investigated structure, after the switching section, an interconnect crossing stage is required to connect the output of the switching sub-networks to the correct output port of the WSS; this stage has been modeled as a frequency-independent loss, with each waveguide crossing introducing 0.05 dB of attenuation; this value has been chosen to represent an optimized solution for the interconnect crossings, compatible with the results present in the literature.[9,10]

3. WDM TRANSPORT LAYER

Having defined the structure and the relevant components, the penalty of the WSS architecture must be characterized in a transmission scenario, enabling the extraction of an impairment model for the higher network simulation. The device implementation was considered for a target application with 24 channels distributed in a 100 GHz DWDM comb, considering three possible output fibers. The channels have been simulated considering dual-polarization 16-QAM modulation format, and a symbol rate $R_s = 60$ GBaud, following the 400ZR standard. No polarization-dependent effects have been considered, assuming an ideal polarization-insensitive response by the components. Due to the computational cost of running DSP-enabled simulations, a device-aware analysis

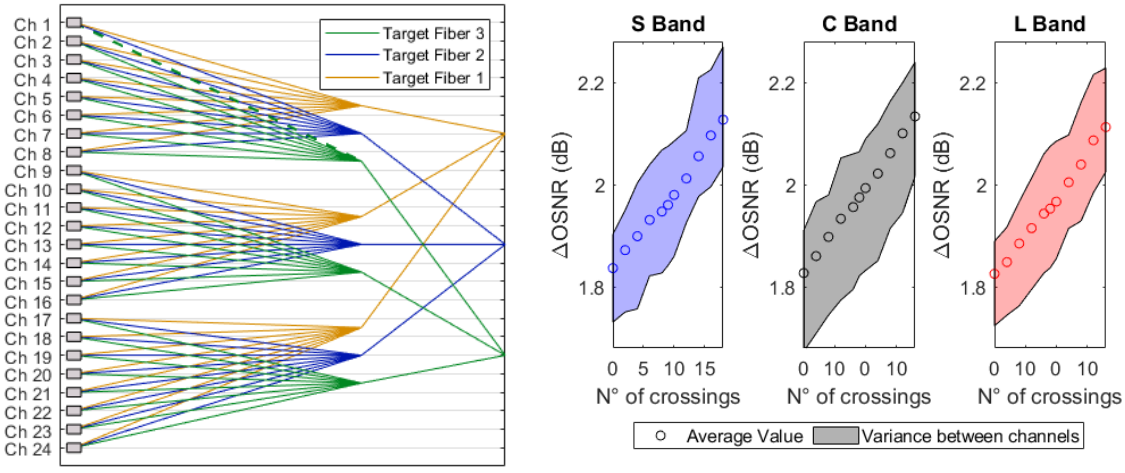

(a) (b)

Figure 2: (a) Topological representation of the interconnect stage and (b) simulated OSNR penalty ($\Delta OSNR$) over the three bands as a function of the encountered number of crossings.

for a realistic band occupation is not feasible, as such the smaller set of 24 channels is simulated to extract the general trend and behavior:[11] the general trend and penalty distribution of the device can be abstracted from the results obtained on this smaller subset. By considering the topology of the interconnection stage and representing the extracted data as a function of the number of encountered crossings (Fig. 2), we can generalize a path-dependant model for an arbitrary scaled device, up to the required number of channels and output ports.

The simulation results are compatible with the scaling assumption as depicted in Fig. 2b. The device operates similarly in the three bands, while the average penalty and channel variation are compatible between the different simulated paths. This model has been used to analytically scale up the device to full spectral occupation and evaluate the additional penalty introduced by the higher number of crossings. This allows a realistic approximation of the penalties expected for a larger implementation, while maintaining the trends and patterns highlighted by the physical-aware device simulations.

4. NETWORKING ANALYSIS

We examined the overall performance of the network to assess the effect of the new WSS architecture on various optical transport methods. We employed the Statistical Network Assessment Process (SNAP) tool, which operates on the network's physical layer and is predicated on the deterioration of Quality-of-transmission (QoT) brought on by each network component.[12]

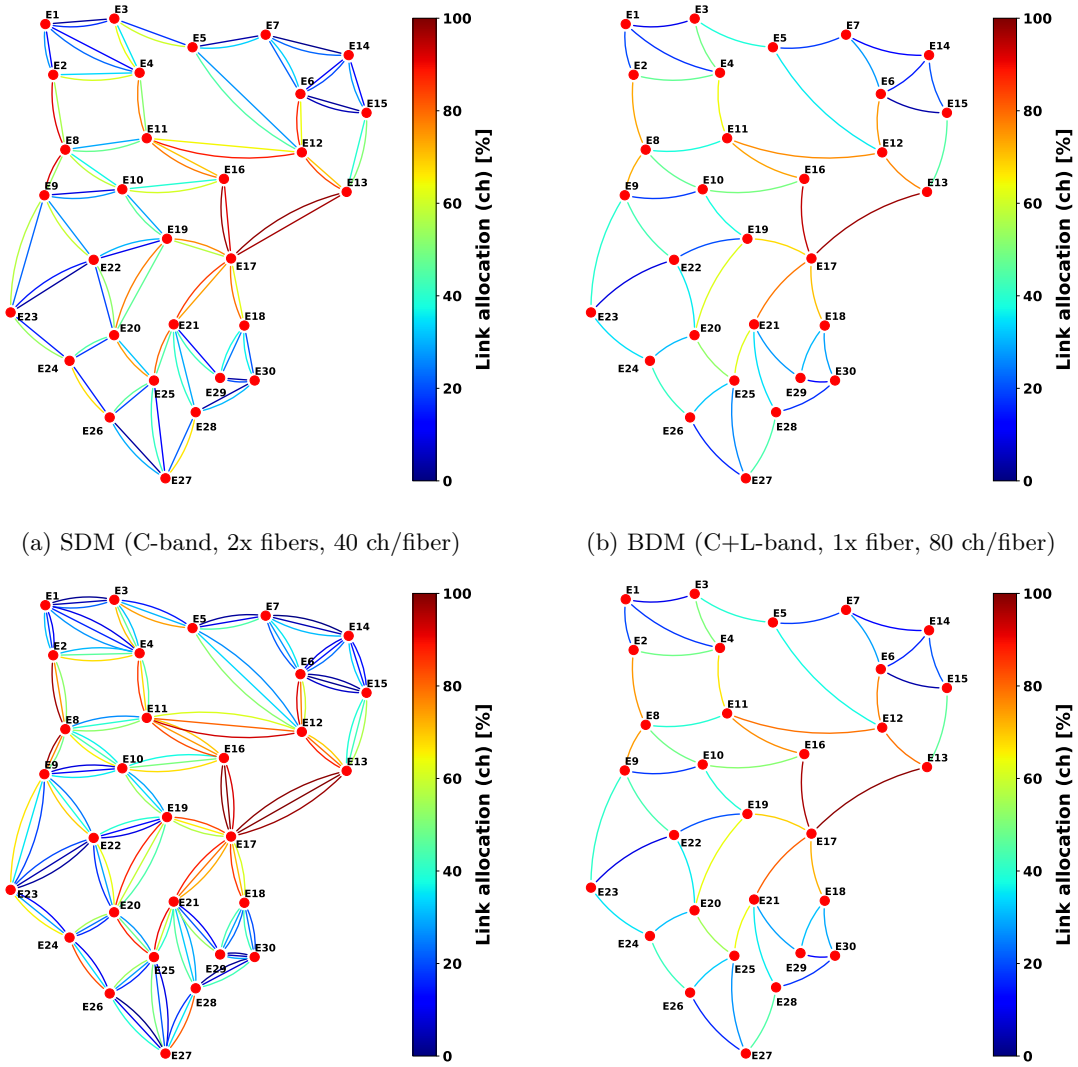

(a) SDM (C-band, 2x fibers, 40 ch/fiber)

(b) BDM (C+L-band, 1x fiber, 80 ch/fiber)

(c) SDM (C-band, 3x fibers, 40 ch/fiber)

(d) BDM (S+C+L-band, 1x fibers, 120 ch/fiber)

Figure 3: Channel allocation comparison - ZR+ transceiver.

We assume a three-band (S+C+L) optical line system with band-optimized network components, including optical amplifiers. We assume that all amplified line fibers are 75 km in length and that standard single-mode fiber is used (ITU-T G.652D). For the C- and L-band channels, we are contemplating the use of commercially available Erbium-doped fiber amplifiers (EDFA), whereas for the S-band, we are contemplating the use of Thulium-doped fiber amplifiers (TDFA). Each band on the ITU-T 100-GHz WDM grid is operated by ZR+ transceivers with a 60 Gbaud symbol rate. In addition, the Routing and Wavelength Allocation (RWA) technique is used to allocate Light-paths (k shortest routes with $k_{max} = 5$ for routing and first-fit for spectrum allocation) (LP). In addition, homogenous network traffic between nodes is used for network evaluation. For the evaluation of the network

performances, we chose the Spain-E topology,[5] comprised of 52 edges and 30 optical nodes, and utilized Monte Carlo analysis to define the network's statistical characteristics.

5. RESULTS AND CONCLUSION

BDM and SDM network performance are compared with the assumption that SDM uses multiple fibers within the C-band on the same total available spectrum in order to facilitate a comparison of the multiband results obtained when the ROADM architecture is utilized in conjunction with the proposed WSS structure. In our investigation, the SDM technique consumes multiples fiber (2x and 3x) compared to the BDM approach. For SDM, we assume a core continuity constraint (CCC), which states that each LP traveling from the source to the destination node must be allocated in the same fiber.[13] Simulations are performed using the allocated channels with a blocking probability of $BP = 10^{-2}$.

In both the SDM with multiple fibers and the BDM situations, the channel allocation (40 channels/band) is analyzed. The comparison between SDM (2x fibers) and BDM (C+L, 80 channels/fiber) is shown in Fig. 3 (a) and (b), while the comparison between SDM (3x fibers) and BDM (S+C+L) is shown in Fig. 3 (c) and (d). A heat map (percentage) showing the channel allocations for each fiber link ranges from 0% (blue) to 100% (orange). In Fig. 3 (a), the SDM scenario (2x fibers, C-band, 40 channels/fiber) has a channel utilization of 41.83%, while the BDM case (1x fiber, CL band, 80 channels/link) in Fig. 3 has a channel utilization of 41.67%. For Fig. 3 (c), the channel utilization is 43.59% for the SDM scenario (3x fibers, just C-band, 40 channels/fiber), however the channel utilization for the entire network is 42.7% for the BDM instance (1x fiber, S+C+L bands, 120 channels/fiber) as shown in Fig. 3 (d).

In both cases, the channel allocation in the BDM scenario is somewhat less than in the SDM scenario, but the gap between SDM and BDM widens in the case of SDM (3x fiber) and BDM (S+C+L bands) due to the non-linear propagation caused by the transmission of all three bands. Compared to the C band scenario, the S+C+L bands instance's capacity was almost tripled. SDM provides superior link allocation than BDM in both scenarios. In any case, the little capacity loss observed in the BDM situation suggests that BDM solutions can be an affordable way to increase network capacity without laying new fibers.

REFERENCES

[1] Kim, K., Doo, K.-H., Lee, H. H., Kim, S., Park, H., Oh, J.-Y., and Chung, H. S., "High speed and low latency passive optical network for 5G wireless systems," *JLT* **37**(12), 2873–2882 (2018).

[2] Ferrari, A., Napoli, A., Fischer, J. K., Costa, N., D'Amico, A., Pedro, J., Forysiak, W., Pincemin, E., Lord, A., Stavdas, A., et al., "Assessment on the achievable throughput of multi-band ITU-T G. 652. D fiber transmission systems," *J. Light. Technol.* **38**(16), 4279–4291 (2020).

[3] Strasser, T. A. and Wagener, J. L., "Wavelength-selective switches for ROADM applications," *IEEE JSTQE* **16**(5), 1150–1157 (2010).

[4] Tunesi, L., Khan, I., Masood, M. U., Ghillino, E., Carena, A., Bardella, P., and Curri, V., "Novel design and operation of photonic- integrated wss for ultra-wideband applications," in [*2022 IEEE Photonics Society Summer Topicals Meeting Series (SUM)*], 1–2 (2022).

[5] Masood, M. U., Khan, I., Tunesi, L., Correia, B., Sadeghi, R., Ghillino, E., Bardella, P., Carena, A., and Curri, V., "Networking analysis of photonics integrated multiband WSS based ROADM architecture," in [*2022 International Conference on Software, Telecommunications and Computer Networks (SoftCOM)*], 1–6, IEEE (2022).

[6] Hammood, M., Mistry, A., Yun, H., Ma, M., Lin, S., Chrostowski, L., and Jaeger, N. A. F., "Broadband, silicon photonic, optical add–drop filters with 3 dB bandwidths up to 11 THz," *Opt. Lett.* **46**, 2738–2741 (Jun 2021).

[7] Masilamani, A. P. and Van, V., "Design and realization of a two-stage microring ladder filter in silicon-on-insulator," *Opt. Express* **20**, 24708–24713 (Oct 2012).

[8] Eid, N., Boeck, R., Jayatilleka, H., Chrostowski, L., Shi, W., and Jaeger, N. A. F., "FSR-free silicon-on-insulator microring resonator based filter with bent contra-directional couplers," *Opt. Express* **24**, 29009–29021 (Dec 2016).

[9] Wu, S., Mu, X., Cheng, L., Mao, S., and Fu, H., "State-of-the-art and perspectives on silicon waveguide crossings: A review," *Micromachines* **11**(3) (2020).

[10] Yi, D., Zhou, W., Zhang, Y., and Tsang, H. K., "Inverse design of multi-band and wideband waveguide crossings," *Opt. Lett.* **46**, 884–887 (Feb 2021).

[11] Khan, I., Tunesi, L., Masood, M. U., Ghillino, E., Carena, A., Bardella, P., and Curri, V., "Performance analysis of novel multi-band photonic-integrated wss operated on 400ZR," in [*2022 IEEE Photonics Society Summer Topicals Meeting Series (SUM)*], 1–2 (2022).

[12] Curri, V., Cantono, M., and Gaudino, R., "Elastic all-optical networks: A new paradigm enabled by the physical layer. how to optimize network performances?," *Journal of Lightwave Technology* **35**(6), 1211–1221 (2017).

[13] Khodashenas, P. S., Rivas-Moscoso, J. M., Siracusa, D., Pederzolli, F., Shariati, B., Klonidis, D., Salvadori, E., and Tomkos, I., "Comparison of spectral and spatial super-channel allocation schemes for SDM networks," *JLT* **34**(11), 2710–2716 (2016).